Published in Construction and Building Materials, 2020, vol. 239, no. 10, article no. 117775, which should be cited to refer to this work.
DOI: https://doi.org/10.1016/j.conbuildmat.2019.117775

Shot-earth for sustainable constructions

A. Curto[a], L. Lanzoni[b,c], A.M. Tarantino[b,c], M. Viviani[a]

[a] *HEIG-VD/HES-SO - Haute Ecole d'Ingénierie et de Gestion du Canton de Vaud, Route de Cheseaux 1, CH-1401 Yverdon*
[b] *DIEF-Department of Engineering "Enzo Ferrari", University of Modena and Reggio Emilia, 41125 Modena, Italy*
[c] *CRICT - Centro Interdipartimentale di Ricerca e per i servizi nel settore delle Costruzioni e del Territorio, University of Modena and Reggio Emilia, 41125 Modena, Italy*

Abstract

Earth has been used worldwide as a building material for centuries and it is still one of the most used construction materials. In many countries the excavated soil is becoming one of the largest construction waste and its disposal is costly and problematic. For this reason, there is a rising interest in employing the excavated soil directly in field, possibly as an added value construction material. In this paper a new type of rammed earth is presented. This new material is based on the shotcrete technology and has been named shot-earth. A mix of stabilized soil, aggregates and water is consolidated by high speed projection rather than by mechanical compaction to obtain both structural and non-structural elements. The first characterization of the physical properties of this material has shown the great potential of this technology.

Keywords: Shot-earth; rammed earth; modern building materials; sustainable constructions.

1. Introduction

Soil has been used to construct for centuries with different methods and technologies. Largely replaced by others materials, the soil is nevertheless still in use in many areas of the world (see Figure 1) and it is still one of the most used construction materials. In many areas of the world, such as

Email address: luca.lanzoni@unimo.it (L. Lanzoni)

France, the soil is particularly adapted to construct because it contains an appropriate quantity of clay. The earth construction has demonstrated to

Figure 1: Diffusion of the raw earth constructions (from [8])

be durable in many contexts as shown by the ancient city of Shibam (see Figure 2a) entirely construed in soil and still populated. Furthermore, many architects have succeeded in using earth to construct modern and durable buildings (see Figure 2b).

(a) Shibam "The Manhattan of the desert" in the 1930s

(b) Rick Joy won the Smithsonian Architecture Design Award with the Tucson Mountain House, Arizona, 2004

Figure 2: Recent constructions realized by using soil as building material

The vernacular construction techniques [7] have evolved such that today are available in the market products such as the "*earth concrete*" [20]. Among

the "*earth concretes*" that have reached a certain popularity there are the Alker and the Cast Earth [40]. Researchers have found a method to produce self-levelling earth concrete based on the use of clayey soil and CSA binders [9, 16]. Many are also the applications of soil placed by projection, most of these are developed for rendering but attempts to constructs walls and houses using projection have been made [3]. Not all the soil is adapted to construct and in these cases other construction techniques have been developed and used (stone and brick masonry, wood, etc.). In other cases the performances of soil have been improved by stabilization [7, 2]. In the past the stabilization of soil was performed by instance by adding straw, rosins and arabic gums while today the stabilization of soil is made by adding binder such as lime, gypsum, different types of cements and magnesium oxides. The high energy compaction methods can also be viewed as a form of stabilization [1]. Stabilization is fundamental to improve a soil that is not adapted for construction and it is widely studied worldwide. In particular, Figure 3 shows that enhancing the mechanical performances (particularly in terms of strength and durability) of crude earth by manipulating its clay fraction might be an effective low-cost approach to avoid various drawbacks linked to the use of Portland as stabilization [20]. Nevertheless, it is remarked that this might be true for clayey soils.

Despite the renewed interest on the soil construction, the codes and practices for structural design remain schematic for vernacular and modern soil-based structures. The technique presented in this paper, named "*shot earthcrete*" or "*shot-earth*" is a new technology based on the high-speed projection (spraying) of a mix of stabilized soil, aggregates and water. Being based on a dry process, the quantity of water in the mix is low and the quantity and type of the stabilization is chosen according to the quality of the excavated soil and the application targeted. Given the lack of norms and codes of practice the characterization of the shot-heart is therefore mandatory in order to understand the behavior of this new material under load. In this research a particular emphasis was paid to the following issues:

− Shot-earthcrete as construction material;
− influence of the placing process on the shot-earthcrete;
− earthcrete as construction technology.

The experimental campaign focused firstly on the identification on the most important mechanical parameters such as ultimate compressive and tensile strengths, Young modulus and Poisson ratio. In a second testing campaign the behavior of the shot earthcrete as a structural material was studied on

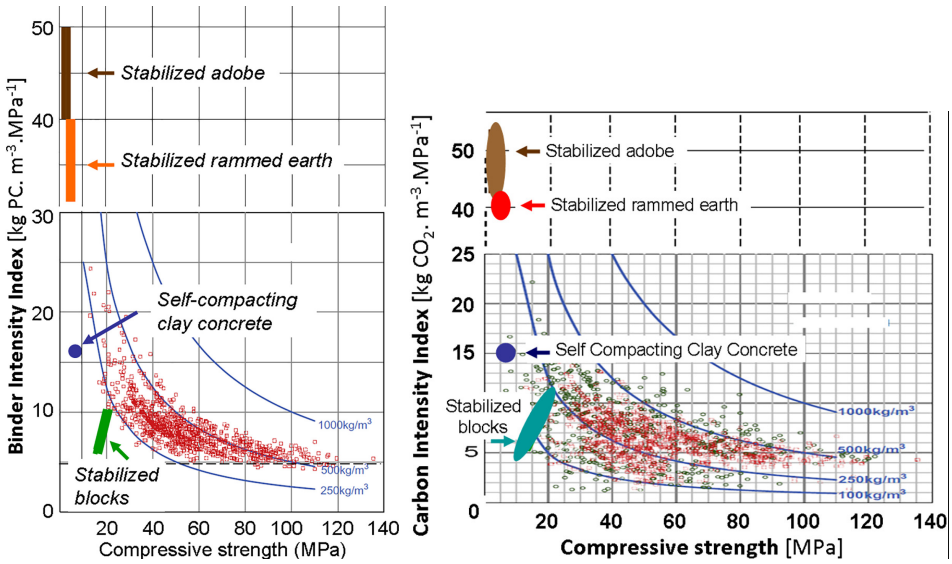

(a) (b)

Figure 3: Effect of stabilization of the earth construction (from [20])

wall-like specimens tested under compression and shear loads.

2. Experimental program

In order to design a load carrying element, some mechanical parameters are needed [21], [22]. For concrete the relationships between many mechanical properties are well known and therefore often it is sufficient the value of the compressive strength to derive most of the other physical properties. The shot-earth can be considered as a low strength concrete but this could not be assumed before testing. Therefore, standard practices for testing concrete and masonry were adopted to determine parameters such as the Young modulus, Poisson ratio, shear modulus and tensile strength [24], [25], [26], [29], [30], [31], [32], [33], [34]. The experimental program consisted of two phases: the first one aimed at testing prismatic specimens; the second one devoted to investigate both axial and diagonal compression of walls samples. All specimens were cured at $23 \pm 1.7°\ C$ $(73 \pm 3°\ F)$ of temperature and $50 \pm 5\%$ of relative humidity and then tested at 28 days. During the drying process the weight loss was monitored with the aid of a thermal camera.

3. Materials and methods

Shot-earth consists of a dry mix of soil, cement and coarse sand (size 0-8 mm) propelled through a nozzle. The size of the sand and the mix design are determined according to the composition of the excavated soil. In this case the mix proportions were 7/7/2 (7 soil, 7 sand and 2 cement) ratio by weight in the dry mixture. This mix was studied to obtain a strength sufficient to construct vaults and walls, without altering the color of the final product. The mixture is pressurized into a properly designed machine and conveyed through a hose to the spraying nozzle by a high velocity air-stream. About 3% (by volume) of water is injected in the nozzle of water to obtain a certain degree of cohesion and promote the hydration of the cement grains. Water has to be added in a quantity that permits adhesion of the mix when shot on the mould and to avoid that the mix do not held in place. Furthermore, water should not be in excess to prevent shrinkage. The projection methodology is fundamental to obtain a good result. Two projection methods were tested, one overhead on a closed mould (see Figure 4b), one on a vertical surface with an angle of approximately 45 (see Figure 4a). The overhead

(a) Shot-earth frontally sprayed

(b) Shot-earth sprayed from overhead

Figure 4: Different methodologies used for casting the shot-earth.

method proved to be the less effective since it promoted a chaotic movement inside the mould with segregation of the mix (see Figure 5b). Furthermore, during the spraying process a cloud of dust formed inside the mold, thus

(a) Coring setup

(b) Segregation in shot-earth specimens

Figure 5: Coring setup and segregation phenomena (overhead projection)

preventing the nozzle-man to see where flow of the material should be directed. The overhead technique is therefore more interesting when used on large horizontal surfaces rather than in vertical closed moulds. None of the above-mentioned problems were encountered while using the side projection method, which was therefore chosen for ensuing phases of the testing campaign.

The machine used to shot the stabilized earth is a modified twin chamber machine, similar to the one showed in Figure 6. This equipment is generally used to shot refractory materials, mixes of dry sand and cement; it is a so-called dry process machine and its production rate equals 10 m^3/hr. This type of dry spray machine is appreciated by practitioners because of its steady rate of feeding into the air stream. This feature allows maintaining a constant water cement ratio and a constant rate of shooting: An unsteady air stream and the ensuing pulsation might cause segregation problem with loss of strength of the material. The dry process also permits to have an excellent green strength since the mixture is well compacted and self-sustaining material as soon as it is placed. Therefore, the surfaces can be immediately finished by hand or mechanically, without risks of damaging the structural elements.

Shot-earth is a method to construct structures and manufacture construction products using soil and also a method to valorize the excavated soil. Basically

(a) Boulder Gun machine used for spraying

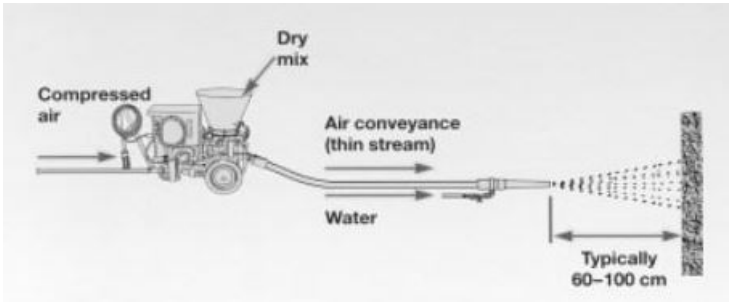

(b) Scheme of the Boulder Gun components

Figure 6: A typical machine for sprayed soil

the soil used in construction should not have a large content of organic matter, therefore 25/50 cm of topsoil should always be removed. The topsoil is also precious for other applications and it should not be damaged or polluted. The presence of pollutants should be checked carefully with techniques such as XRF, XRD and other chemical analyses. Furthermore, the excavated soil should be let dry and then undergoes through a sieving and screening process. Sieving and screening allows removing all aggregates present in the soil and screening will help to obtain an optimal size of the soil particles. Gravel and soil thus obtained are then used to formulate the mix of the shot-earth. In this case a cement CEM I 42.5N was used for stabilization.

4. Specimens

For this testing campaign several specimens were manufactured ([23], [27]) and, in particular, two large walls (1 x 1 x 0.3 m^3) were prepared in order to check the projection method (head on or side) and to extract cores (see Figure 5a) for direct traction test, thus assessing the quality of the material. Specimen sizes and their use are listed in Table 1.

The drying process of specimens was monitored by means of weighting and by means of thermal camera images (see Figure 7). The drying process of the specimens was carried out at $20 \pm 2°C$ of temperature and $50 \pm 5\%$ of relative humidity (RH). The specimen weight was monitored using an electronic scale. Figure 8 illustrates the weight loss in time in order to describe the drying process and the shot-earth curing: From the shot-earth casting, approximately 20 days elapsed before achieving a constant weight of about 132 kg. Therefore the specimen lost around 6.4 kg as the result of drying process [28]. The shot-earth walls manufactured had a bulk density of about 2070 kg/m^3.

5. Results and discussion

5.1. Compressive Test

The compressive strength was determined by using standard test procedure for concrete. In fact this shot-earth mix has shown mechanical properties that resemble those of a low strength concrete.
The machine used for this test was a W+B LFV 200 kN apparatus (see Figure 10). The compressive test was carried out on five 15 x 15 x 15 cm^3 cubes cured for 28 days. The strength values are listed in Table 2. The failure mode, characterized by the formation of a cone, is admitted by codes and in general the specimens have a brittle failure after achieving their maximum compressive stress (see Figure 9).

5.2. Young Modulus

Young modulus was determined according to EN 12390-13 [36]. The test method allows determining two moduli of elasticity: The initial modulus $E_{c,0}$ measured at first loading, and the stabilized modulus $E_{c,s}$ measured after three loading cycles (see Figure 11). The strain evaluation was based on the ϵ curve, with three repetition of loading for measuring the time effect.

Specimen	Test	Regulation
Wall 1 x 1 x 0.3 m^3	Direct traction on cores Compressive strength on cores. Visual detection of the quality of the material. Evolution of drying.	UNI 6135 EN 12390-13 UNI EN 12390-1
Wall 0.8 x 0.8 x 0.1 m^3 unreinforced	Compression test on the specimen	–
Wall 0.8 x 0.8 x 0.1 m^3 reinforced	Compression test on the specimen	–
Wall 0.5 x 0.5 x 0.11 m^3	Diagonal compression test	ASTM E519/E519M-15
Cube 0.15 x 0.15 x 0.15 m^3	Compressive strength	UNI EN 12390-1 UNI EN 12390-2 UNI EN 12390-3
Prism 0.12 x 0.12 x 0.36 m^3	Elastic modulus	UNI EN 12390-5 UNI 6133 ASTM-C293 2016
Cube 0.15 x 0.15 x 0.15 m^3	Poisson ratio	–
Prism 0.12 x 0.12 x 0.36 m^3	Shear strength and shear modulus	ASTM E519-15

Table 1: Experimental tests carried out on specimens.

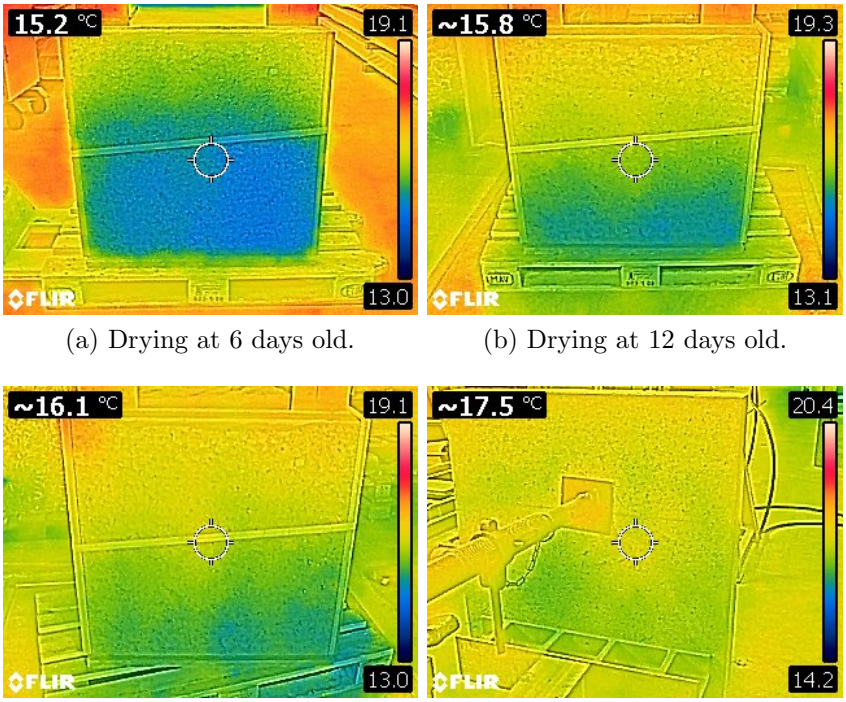

(a) Drying at 6 days old.

(b) Drying at 12 days old.

(c) Drying at 18 days old.

(d) Drying at 28 days old.

Figure 7: Drying process of the unreinforced wall

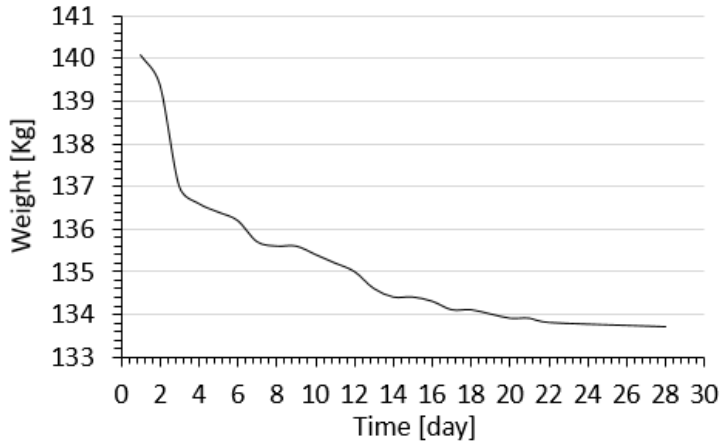

Figure 8: Drying process: Relation between weight loss and curing time

Specimen	σ_c $[MPa]$
$SE-ACT1$	9.058
$SE-ACT2$	9.698
$SE-ACT3$	10.120
$SE-ACT4$	10.373
$SE-ACT5$	8.258
Average	9.501
$COV\%$	9

Table 2: Compressive strength

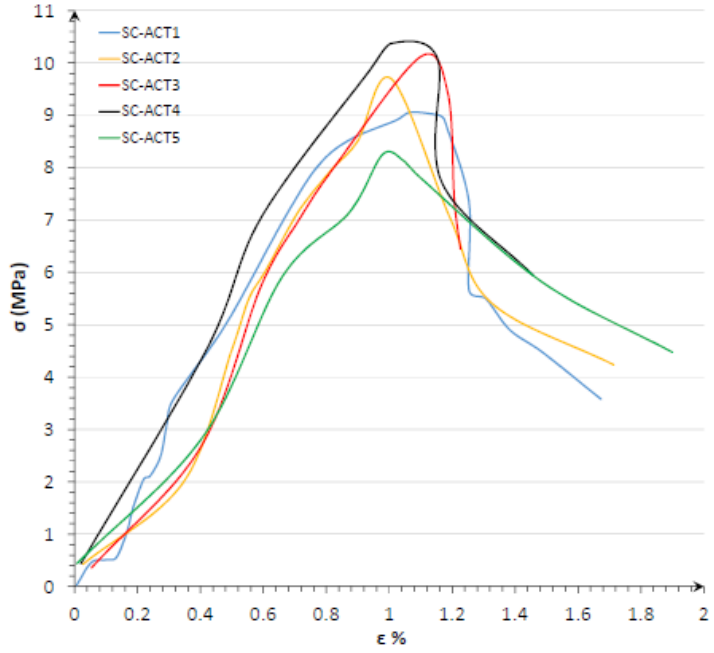

Figure 9: $\sigma - \epsilon$ behavior under compression

The $E_{c,s}$ corresponds to the secant slope passing through the origin and to the ordinate point 0.33 σ_c [1], namely $E_{c,s} = \sigma_{1/3}/\epsilon_{1/3}$.

Results listed in Table 3 shown the stabilized Young modulus, which was

[1] σ_c denotes the ultimate compressive strength.

Figure 10: Compression test setup

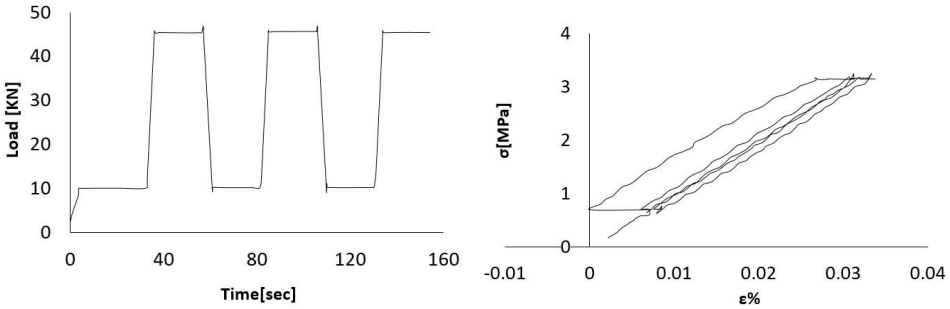

(a) Load-Time graphic (b) Stress-Strain cycles

Figure 11: Evaluation of the Young modulus

computed between 5 and 33% of σ_c by linear fitting; it showed relatively low scattering and $E_{c,s}$ varied between 9638 and 11980 MPa; R^2 is the proportion of the variance in the dependent variable predictable from the independent variable(s). Stress-strain curves and line of linear regression are depicted in Figure 12. The linear regression is a linear approach for modelling the relationship between scalars. The slope of the trend line represents the Young modulus, $E_{c,s}(lr)$ obtained by linear regression.

Specimen	$E_{c,s}$ $[MPa]$
$SE-YM1$	10521
$SE-YM2$	11980
$SE-YM3$	9638
$SE-YM4$	11793
$SE-YM5$	10639
$SE-YM6$	11366
$Average$	10990
$COV\%$	8
$E_{c,s}(lr)$	9707
$R^2\%$	88

Table 3: Young moduli $E_{c,s}$: Young modulus obtained by linear regression $E_{c,s}(lr)$; Covariance COV%; Coefficient of determination $R^2\%$

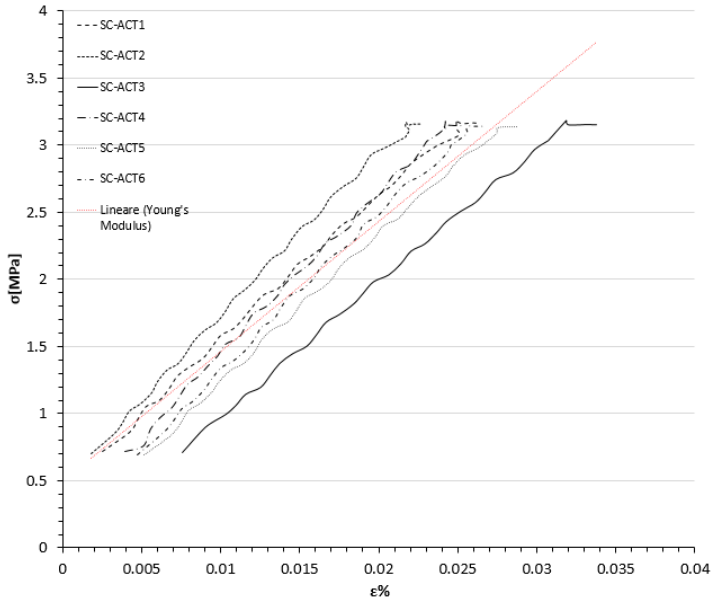

Figure 12: Stress-strain curves and trend line for the Young modulus

5.3. Poisson ratio

For evaluating the Poisson ratio, two transducers were placed orthogonally to the load direction and on the opposite cube sides were used for

Specimen	ν
$SE-PR1$	0.1588
$SE-PR2$	0.1235
$SE-PR3$	0.1815
Average	0.1546
$COV\%$	22

Table 4: Poisson ratio

measuring both the transverse and longitudinal strains ϵ_t, ϵ_l (see Figure 13).

The load system was set in displacement control with repetition of three cycles of loading and unloading (for the time effect), assuming to be in linear field and considering the range up to 0.33 σ_c. The determined values of the Poisson ratio are listed in Table 4. It should be noted that ν showed high scattering because values varied between 0.1235 and 0.1815. The rison of this relatively high scattering of the Poisson ratio lies in the progressive breakdown of the specimen as the load increases.

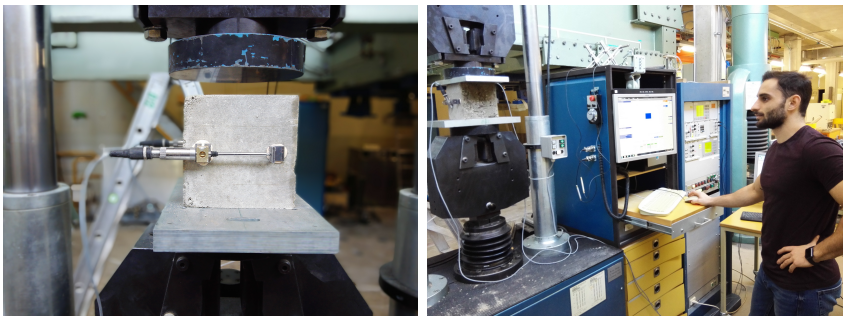

(a) Transducer disposition for the lateral strains

(b) Set-up machine

Figure 13: Machine setting to evaluate the Poisson ratio

5.4. Direct tensile test

Under a direct tensile load test, the shot-earth has shown an elastic-brittle behavior, thus the tensile branch may be well described by a linear constitutive law until the brittle failure according to the classical formula $\sigma_{ct}(\epsilon) = E_{ct}\,\epsilon$, being E_{ct} the elastic modulus of the soil-cement mixture (after curing) and ϵ is the axial strain. The direct tensile strength test consists of applying an increasing traction force until complete failure. Under pure traction load, the tensile strength value is measured as the ratio between the applied load and specimen area. The direct tensile strength test provides more representative values than the flexural tests. Three shot-earth cylinders of 150 *mm* in diameter and 300 *mm* height, cored from existing walls, were tested under direct traction. The average strength of the specimen was of about 11 *MPa*. Because of the notch, the middle cross section was reduced by 26%, see Figure 14[2]. The stress σ_{ct} was calculated as the ratio between the applied tensile load and the area of the notched cross section of the specimen. Table 5 summarizes the mechanical properties of the shot-earth

(a) Cross section reducing (b) Load application for direct tensile test

Figure 14: Direct tensile test set-up

[2]The depth of the notch is approximately 10 *mm*, thus the reduced area of the cross section turns out to be $\pi 140^2/4 \cong 13273\,mm^2$.

Specimen	$\sigma_{ct}[MPa]$
$SE-DT1$	1.057
$SE-DT2$	1.299
$SE-DT3$	1.120
Average	1.159
$COV\%$	10

Table 5: Direct tensile strength

obtained from direct tensile tests. The average strength was found to be 1.159 *MPa*. Two extensometers with a gauge length of 38 *mm* were set to measure the longitudinal displacements.

The Figure 15 shows the stress-strain curve of the specimen under direct tensile test.

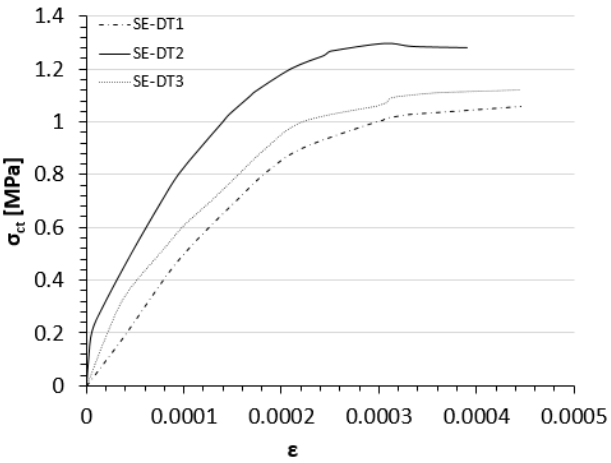

Figure 15: Stress-strain curve provided by direct tensile test

5.5. Three points flexural test

In measuring the tensile strengths of brittle materials, the direct test method might be difficult to implement, inaccurate and costly [39]. These are the reasons why, when a material is already well known, the indirect tensile test is often used for quality control and characterization purposes. A typical three-point loading bending test [37] set-up is shown in Figure 16. The maximum bending tensile stress is calculated under the assumption

Figure 16: Bending test setup

that the neutral axis is at mid-height of the cross-section and the stress distribution is triangular. The modulus of rupture, that is also defined as the bending tensile strength [38], can be measured using the classical formula $\sigma_{ct} = (h/2)\, M_{max}/J_x = 3FL/(2bh^2)$.

Table 6 summarizes the flexural modulus of rupture of the shot-earth specimens. It should be noted that σ_{ct} shows relatively low scattering and it varied between 2.281-1.759 *MPa*. Tensile strengths obtained by indirect tensile test is higher, by a factor of two or more, than those obtained by the conventional direct test [39].

5.6. Evaluation of experimental results

Analyzing the compression stress-strain diagram up to a third of the strength, the behavior of the material can be considered as linearly elastic.

Specimen	σ_{cft} $[MPa]$
$SE-BT1$	1.759
$SE-BT2$	1.993
$SE-BT3$	2.281
$SE-BT4$	1.817
$SE-BT5$	2.207
$SE-BT6$	2.165
Average	2.037
$COV\%$	11

Table 6: Tensile strength σ_{cft} provided by bending test

At σ_c equal to 70% of the maximum compressive strength, the curvature increases rapidly (hardening) and, after achieving the maximum stress, the diagram shows a softening branch until the failure point, as depicted in Figure 9. A loosening of the internal structure and an increase of the transverse strain is recorded after the stress reaches 0.7 σ_c.

The tensile strength of soil-cement depends by the test method. The values of the direct tensile strength recorded during this test campaign are coherent with those reported in literature [35]. The ratio between tensile and compressive strengths is about $1:8$ as shown in Table 7.

In summary it is possible to affirm that the shot-earth tested has the mechanical characteristics of a low strength concrete (see Table 7). It is, however, necessary to highlight the fact that the concrete-like behavior of the shot earth must be further confirmed, in order to safely use the RC concrete design practices for calculating the shot earth elements. This could also lead to applying the same strengthening and maintenance strategies used for concrete to shot earth structures [13].

Type of test	*Average result*
Compressive strength, σ_c	9.501 $[MPa]$
Young modulus, $E_{c,s}$	9707 $[MPa]$
Poisson ratio, ν	0.1546
Direct tensile strength, σ_{ct}	1.159 $[MPa]$
Flexural strength, σ_{cft}	2.037 $[MPa]$

Table 7: Summary of testing result for shot-earth.

6. Walls

The data of the first test campaign on walls highlighted that the frontally spraying methodology yields the best results and therefore this placing method was retained. Three walls were prepared and tested, two under axial compression and one under diagonal compression.

The two walls tested under compression were designed with the dimension of $800\times800\times100$ mm^3 and one of them was reinforced by a steel mesh in each side. The third wall was manufactured with the dimension of $500\times500\times110$ mm^3 according to ASTM E519/E519M-15, the standard test method for diagonal tension [33].

6.1. Axial compression test of walls

Before testing the walls under compression, the top surface was rectified by a rapid set cement mortar. The load applied to the specimen was distributed with a steel profile placed at the top surface. Linear variable differential transducers (LVDT) with a gauge length of 250 mm were placed on both faces of the specimen for measuring both longitudinal and lateral displacements. The geometry of the supports and disposition of LVDTs are shown in Figure 17. The axial stress-strain curve (see Figure 18) for the unreinforced shot-earth wall has shown a linear behavior in the first part and then a progressive decrease in stiffness until the maximum load of about 756 kN was achieved. The modulus of elasticity E equals to about 4418 MPa and it was computed on the range $5\% \div 30\%$ of σ_c. In general the wall exhibited a brittle failure in short time after achieving the maximum compressive stress. As depicted in Figure 18, the positive values represent longitudinal strain and the negative values represent transverse strain.

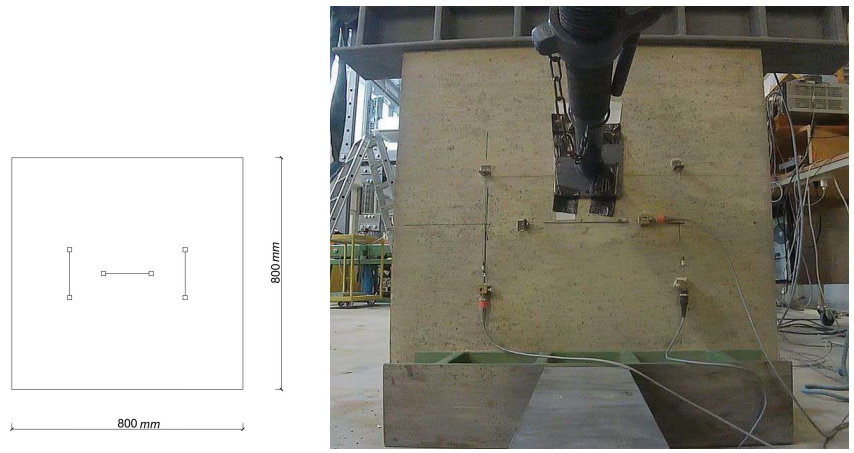

(a) Geometry of the LVDTs disposition

(b) Compression test

Figure 17: Geometry set-up and disposition of transducers

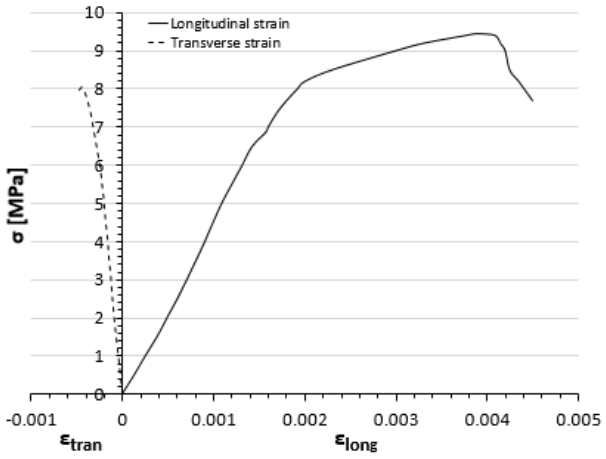

Figure 18: Stress-strain curve of unreinforced wall tested under compression.

The reinforced wall was manufactured for the sole purpose of evaluating the shot-earth behavior with steel reinforcements in terms of technology application, workability and soil-cement/steel interface. Regarding the reinforced wall, the failure occurred without achieving the maximum compressive strength due to the concrete cover debonding and the buckling of steel rebars. This is the reason because the wall without reinforcements exhibited

an ultimate load (756 kN) greater than that achieved by the reinforced wall (equal to 623 kN). The axial stress-strain curve for the reinforced shot-earth wall (see Figure 19) is still in the elastic branch with a Young modulus of 7406 MPa and with axial deformations in the range of $0.01 - 0.1\%$ before failure.

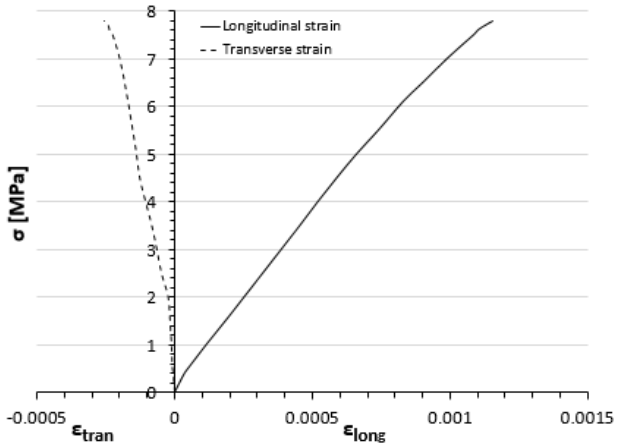

Figure 19: Stress-strain curve of reinforced wall tested under compression

	Unreinforced wall	Reinforced wall
F_c, maximum load $[kN]$	756	623
σ_c, compressive strength $[MPa]$	9.46	7.79
E, Young modulus $[MPa]$	4418.7	7406
ν, Poisson ratio	0.18	0.16

Table 8: Results of the axial compression test

Table 8 summarizes the mechanical properties of both walls tested under axial compression. In general the unreinforced walls exhibited a brittle failure in a short time after achieving the maximum compressive load. In the elastic field, the reinforced wall has shown greater axial rigidity since the beginning of the test, and this highlights that the steel reinforcement could improve the shot-earth performance. By analyzing the broken specimens it is evident that the shot-earth did not has any problems to get through the steel cage and no segregation effect occurred (see Figure 20).

Figure 20: Failure of the reinforced wall

6.2. Diagonal compression test

This test method was developed to measure more accurately the diagonal tensile strength by loading the wall in compression along one diagonal, thus inducing a diagonal tension failure with the specimen splitting apart parallel to the direction of load.
The diagonal compression test was performed according to the ASTM E519-15 [33]. The test set-up provides the layout of a compression load piston on the top surface with a maximum load of 300 *kN*. Two linear differential transducers (LVDT) were placed along the diagonals of both faces of the specimen as showed in Figure 21. The test was carried out under displacement control at a rate of 0.6 *mm/s*. The purpose of the diagonal compression

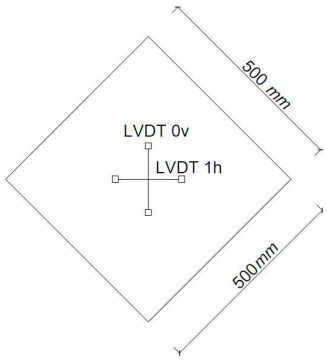

(a) Geometry of the LVDTs disposition. LVDT 5v and LVDT 6h are placed in the hidden side of the sample, thus they are not shown in the figure

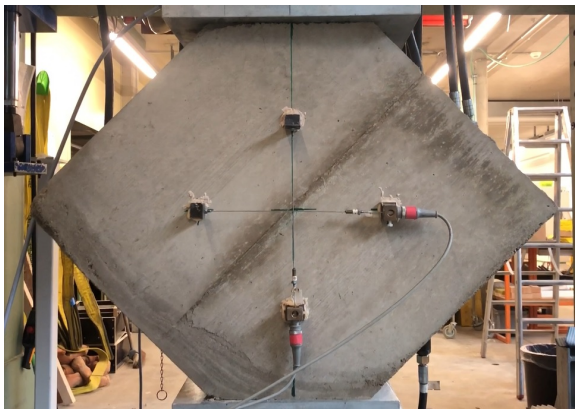

(b) Diagonal compression test

Figure 21: Geometry of the test setup and LVDTs disposal

test is to identify the shear mechanical parameters such as the ultimate shear strength τ and the shear modulus G. While shear modulus measurements are considered accurate, the measure of the shear strength is more complex. The presence of non-pure shear loading, non linear behavior, edges, material coupling and presence of normal stresses make questionable the evaluation of the shear strength.

However, according to [33], the shear stress τ can be calculated as

$$\tau = \frac{0.707P}{A}, \tag{1}$$

being P is the load applied to the wall and A is the area of the specimen. The shear strain is calculated as follows:

$$\gamma = \frac{\Delta v}{g} + \frac{\Delta h}{g}, \tag{2}$$

where γ is the shearing strain, Δv is the vertical shortening, Δh is the horizontal extension and g is the gage length. Accordingly, the shear modulus turns out to be $G = \tau/\gamma$. Figure 22 displays the shear stress-strain curve of the wall whereas Figure 23 shows the diagonal deformation during time.

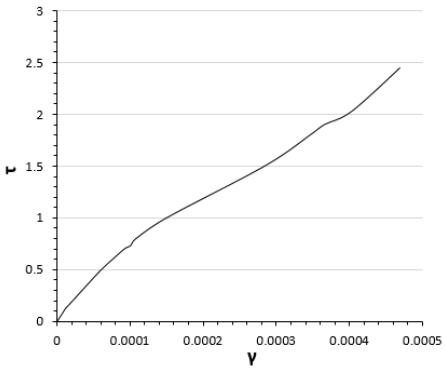

Figure 22: Shear-stress curve of a wall-like specimen under diagonal compression

	Specimen
P, maximal load $[kN]$	191
τ, shear stress $[MPa]$	2.45
G, shear modulus $[MPa]$	5981

Table 9: Results of the diagonal compression test

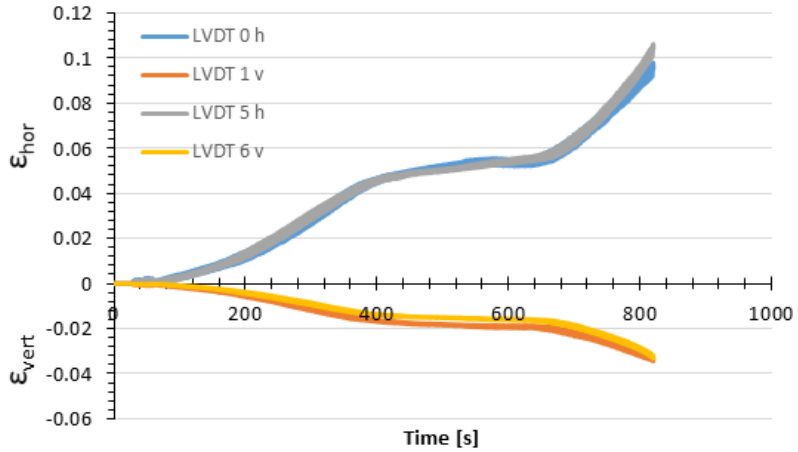

Figure 23: Strain-time curve (the LVDTs disposition is shown in Figure 21a)

The shear mechanical parameters are listed in Table 9. Assuming an elastic behavior of the material, G was measured between the 5 and 33% of τ. Failure of the specimen was preceded by the appearance and consecutive propagation of a crack that crossed diagonally the specimen as showed in Figures 24a-b. Just before collapse, a system of running cracks developed, thus causing the complete failure[3].

[3]Recent works concerning the modeling of damage at large deformations can be found in [11, 12, 14].

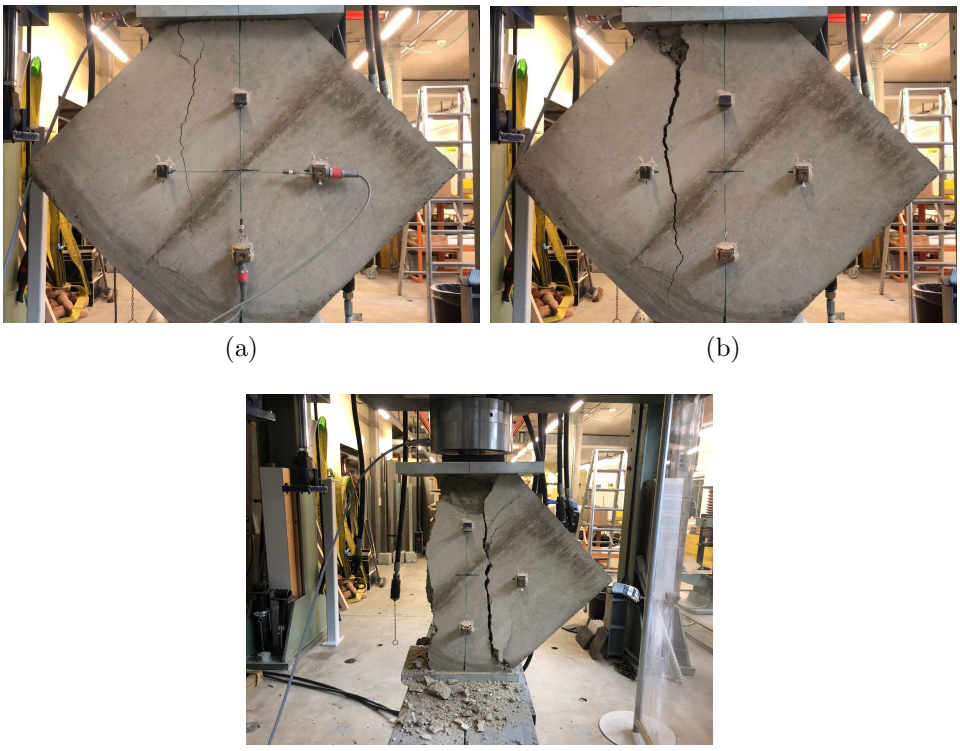

(a) (b)

(c)

Figure 24: Cracks pattern in a shot-earth wall tested under diagonal compression

7. Conclusion

The shot-earth is a new and sustainable construction material consisting in a mix of excavated soil, sand and water placed by high speed projection (dry process). In this case the shot earth was stabilized in order to improve its mechanical properties. The construction material obtained reveals good mechanical properties, which resemble those of a low-strength concrete. The shot-earth spraying technology is very flexible and adapted to a wide range of non-structural and structural applications such as curved, free-formed and form-resistant structures. The experimental investigation accomplished in this work leads to the following main conclusions:

- Excavated soil can be used as a construction material provided that its characteristics are known and a proper stabilization is used;

- the high-speed projection allows for optimal compaction and homogeneity of the material, provided that the projection is performed frontally on an open mould;
- it might be argued that the mechanical behavior of shot-earth is similar to that of a low strength concrete;
- the stabilization rate and type can be changed in order to fit the specificity of each application of this new material;
- the shot-earth increases the sustainability and circularity of the construction market by using a high rate of excavated soil in field, thus reducing the logistic and the supply of other construction materials.

Further studies are carried out to corroborate the results achieved in the present paper and to investigate other properties such as the shrinkage, creep and durability of this innovative material[4].

Acknowledgements

Authors gratefully acknowledge the financial support provided by HEIG-VD / HES-SO under the frame of the projects *Terre 2020* and *Next Earth building*. Financial support from the Italian Ministry of Education, University and Research (MIUR) in the framework of the Project PRIN "*Modelling of constitutive laws for traditional and innovative building materials*" (code 2017HFPKZY) is gratefully acknowledged.
The authors are grateful to the firm Pittet Artisans sárl for their support in manufacturing the specimens and optimizing the shot earth mix.

References

[1] Bruno AW, Gallipoli D, Perlot C, Mendes J. *Mechanical behaviour of hypercompacted earth for building construction*. Mater. Struct. **50** (2017) 160.

[4]The mechanical behavior of rammed earth could be improved by inserting fibres into the mixture at the mixing stage. Recent works about cementitious composites reinforced by a steel fabric or discrete fibres be found in [4, 5] and [17, 18, 19, 10, 15], respectively. Possible applications to improve the building foundations could be investigated too [6].

[2] Bui QB, Morel J-C, Venkatarama Reddy BV, Ghayad W. *Durability of rammed earth walls exposed for 20 years to natural weathering*. Build. Environ., **44** (2009), 912-919.

[3] Easton D. *Modern Earth Buildings*. In: R.L. and M.K. Matthew R. Hall (Ed.), Mod. Earth Build. Mater. Eng. Constr. Appl. (2012) 385400.

[4] Falope FO, Lanzoni L, Tarantino AM. *Double lap shear test on steel fabric reinforced cementitious matrix (SFRCM)*. Composite Structures **201** (2018) 503-513.

[5] Falope FO, Lanzoni L, Tarantino AM. *Modified hinged beam test on steel fabric reinforced cementitious matrix (SFRCM)*. Composites Part B **146** (2018) 232-243.

[6] Forcellini D, Tarantino AM. *Assessment of stone columns as a mitigation technique of liquefaction-induced effects during Italian earthquakes (may 2012)*. The Scientific World Journal **8** (2014), Article ID 216278.

[7] H. Houben, H. and Guillaud. *Earth construction: a comprehensive guide*. Habitat International **19**(4) (1995) 643-644.

[8] H. Houben, H. Guillaud. *Trait de Construction en Terre*, Parenthse, CRATerre, 2014

[9] Landrou G, Ouellet-Plamondon CM, Brumaud C, Habert G. *Development of a self-compacted clay-based concrete: rheological, mechanical and environmental investigations*. World, SB**14** (2014), 10.13140/2.1.1054.2401

[10] Lanzoni L, Nobili A, Tarantino AM. *Performance evaluation of a polypropylene-based draw-wired fibre for concrete structures*. Construct. Build. Mater. **28** (2012) 798-806.

[11] Lanzoni L, Tarantino AM. *Damaged hyperelastic membranes*. Int. J. NonLinear Mech. **60** (2014) 9-22.

[12] Lanzoni L, Tarantino AM. *Equilibrium configurations and stability of a damaged body under uniaxial tractions*. ZAMP Zeitsc. Angew. Math. Phys. **66**(1) (2015) 171-190.

[13] Lanzoni L, Soragni M, Tarantino AM, Viviani M. *Concrete beams stiffened by polymer-based mortar layers: Experimental investigation and modeling*. Construction and Building Materials **105** (2016) 321-335.

[14] Lanzoni L, Tarantino AM. *A simple nonlinear model to simulate the localized necking and neck propagation*. Int. J. NonLinear Mech. **84** (2016) 94-104.

[15] Nobili A, Lanzoni L, Tarantino AM. *Experimental investigation and monitoring of a polypropylene-based fiber reinforced concrete road pavement*. Construct. Build. Mater. **47** (2013) 888-895.

[16] Ouellet-Plamondon CM, Habert G. *Self-Compacted Clay based Concrete (SCCC): Proof-of-concept*. J. Clean. Prod. **117** (2016) 160-168

[17] Savino V, Lanzoni L, Tarantino AM, Viviani M. *An extended model to predict the compressive, tensile and flexural strengths of HPFRCs and UHPFRCs: Definition and experimental validation*. Composites Part B **163** (2019) 681689.

[18] Savino V, Lanzoni L, Tarantino AM, Viviani M. *Tensile constitutive behavior of high and ultra-high performance fibre-reinforced-concretes*. Construction and Building Materials **186** (2018) 525-536.

[19] Savino V, Lanzoni L, Tarantino AM, Viviani M. *Simple and effective models to predict the compressive and tensile strength of HPFRC as the steelfiber content and type changes*. Composites Part B **137** (2018) 153-162.

[20] Van Damme H, Houben H. *Earth Concrete. Stabilization Revisited*. Cem. Concr. Res. **114** (2017) 90-102.

[21] Vanderwalle L. et al. Recommendation of Rilem TC162-TDF. *Test and design methods for steel fibre reinforced concrete. Design of steel fibre reinforced concrete using the s-w method: principles and applications*. Materials and Structures **35** (2002) 262-278

[22] ACI Committee 544. *ACI 544.4R88* Design consideration for steel Fiber Reinforced Concrete. ACI 544.4R-88America Concrete Institute. ACI Farmington Hills, MI 1996

[23] CNR-DT 204. *Guidelines for design, construction and production control of fiber reinforced concrete structures.* National Research Council (CNR) of Italy 2006

[24] ACI Committee 318. *Report ACI 31808/318R-08.* Building code and commentary. Report ACI 318-08/318R-08 American Concrete Institute, Farmington Hills, MI, 2008

[25] UNI EN 206-1. *Concrete Part 1: Specification, performance, production and conformity* 2006

[26] UNI EN 12390-3. *Testing hardened concrete Compressive strength of test specimens* 2003

[27] PrSIA 2052. *Béton fibré ultra-performant (BFUP)-Matériaux, dimensionnement et exécution* 2015-05

[28] Brite-Euram Project BRPRCT980813. *Test and Design methods for Steel Fibre Reinforced Concrete* 2001

[29] EN 1992-1-1. *Design of concrete structures General rules and rules for buildings* 1992

[30] UNI EN 12390-1. *Testing hardened concrete. Shape, dimensions and other requirements for specimens and moulds* 2012

[31] UNI EN 12390-5. *Testing hardened concrete. Flexural strength of test specimens* 2009

[32] UNI 6133. *Measuring the flexural tensile strength*

[33] ASTM E519/E519M-15. *Standard test method for diagonal tension (shear) in masonry assemblages*

[34] UNI 6135. *Standard test method for direct tensile strength*

[35] Hongxia Yang. *Experimental Study on Mechanical Property of Soil-Cement-Department of Civil Engineering, Shandong Jiaotong University, 2012*

[36] EN 12390-13. *Testing hardened concrete. Determination of secant modulus of elasticity in compression*

[37] ASTM-C293 2016. *American Society for Testing and Materials. International-Standard test method for flexural strength of concrete*

[38] Flexural strengths. *J.T.Balbo. Relations between indirect tensile and flexural strengths for dry and plastic concretes. IBRACON Estrut. Mater. vol.6 no.6, Dec. 2013.*

[39] Measurement of the tensile strength. *American Society for Testing and Materials A.R.C.S. R. BERENBAUM, Ph.D. and I. BRODIE. Measurement of the tensile strength of brittle materials. Mining Research Establishment, National Coal Board, Worton Hall, Isleworth, Middlesex, 9 October, 1958.*

[40] *Cast earth* (n.d.). www.greenhomebuilding.com

List of Figures